Available online at www.sciencedirect.com
ScienceDirect
International Journal of Plasticity 23 (2007) 227–243
INTERNATIONAL JOURNAL OF Plasticity
www.elsevier.com/locate/ijplas

Role of strain-rate sensitivity in the crystal plasticity of hexagonal structures

Benoît Beausir [a,b], László S. Tóth [a,*], Kenneth W. Neale [b]

[a] *Laboratoire de Physique et Mécanique des Matériaux, Université de Metz, Ile du Saulcy, 57045 Metz, France*
[b] *Faculté de génie, Université de Sherbrooke, Sherbrooke, Que., Canada J1K 2R1*

Received 13 November 2005
Available online 22 August 2006

Abstract

In the first part of this paper the stress and strain-rate response of hexagonal crystal structures are examined when slip is viscoplastic according to a power law. The stress and strain-rate equi-potential surfaces are constructed and discussed as a function of the strain-rate sensitivity index m. The second part of this paper deals with the case of linear viscous slip; i.e., for the case when m is equal to one. A simple analytic solution is presented to obtain the deviatoric stress state for a given strain-rate. It is shown that the plastic spin is *not* zero for $m = 1$ in hexagonal crystal structures, contrary to the cubic case where the plastic spin vanishes. In addition, the rate of texture evolution in simple shear of a magnesium polycrystal is examined as a function of m.

Keywords: Crystal plasticity; Strain-rate sensitivity; Plastic spin; Hexagonal; Viscous slip

1. Introduction and basic equations

A common problem that often arises in crystal plasticity is to obtain the stress state that corresponds to a given imposed strain-rate. In time-independent plasticity and when the Schmid law is used, the solution can be obtained using the maximum work principle with the help of the vertices of the Bishop and Hill yield surface (Bishop and Hill, 1951). The procedure consists of calculating the plastic power corresponding to 56 stress states (for

* Corresponding author. Tel.: +33 387547238; fax: +33 387315366.
E-mail address: toth@univ-metz.fr (L.S. Tóth).

0749-6419/$ - see front matter © 2006 Elsevier Ltd. All rights reserved.
doi:10.1016/j.ijplas.2006.02.013

fcc crystal structures) defined by the vertices, and then locating the vertex that corresponds to the maximum plastic power. The procedure fails, however, when the imposed strain-rate vector is perpendicular to a hyperplane of the yield surface, because several vertices give the same maximum plastic power. This is referred to as the stress ambiguity problem in rate-independent plasticity. When the strain-rate is not perpendicular to any of the hyperplanes, another ambiguity problem arises which concerns the selection of the active slip systems as there are too many (6 or 8 at the vertices). These problems do not occur with rate-dependent plastic slip with a constitutive law of the form (Hutchinson, 1976):

$$\tau^{s,f} = \tau_0^f \operatorname{sgn}(\dot{\gamma}^{s,f}) \left| \frac{\dot{\gamma}^{s,f}}{\dot{\gamma}_0} \right|^m = \tau_0^f \frac{\dot{\gamma}^{s,f}}{\dot{\gamma}_0} \left| \frac{\dot{\gamma}^{s,f}}{\dot{\gamma}_0} \right|^{m-1}. \tag{1}$$

Here $\tau^{s,f}$ is the resolved shear stress in the slip system indexed by s of the family indexed by f, $\dot{\gamma}^{s,f}$ is the slip rate, the τ_0^f value is the reference stress level (at which the slip rate is $\dot{\gamma}_0$), and m is the strain-rate sensitivity index. The reference shear rate $\dot{\gamma}_0$ is supposed to be constant for all slip systems. The slip systems are grouped into "families" for which purpose the index f will be used hereafter. The main families in hexagonal structures are the basal, prismatic and pyramidal slips. It is assumed here that the reference shear stress τ_0^f is the same for a given slip system family, but can be different from one family to another. Eq. (1) has been widely used in crystal plasticity simulations (e.g., Asaro and Needleman, 1985; Tóth et al., 1988, 1990; Neale et al., 1990; Van der Giessen et al., 1992).

The properties of the stress potential function that corresponds to Eq. (1) have been analysed by Tóth et al. (1988) for cubic structures, where it has been shown that the stress potential surfaces are smooth, convex, and more and more rounded when the m value is increased. The first part of this paper presents a similar analysis for hexagonal structures, where the potentials depend not only on the m value but also on the relative strengths of the different slip system families as well as on the hexagonal lattice parameter c/a.

In viscoplastic slip, in order to obtain the stress state that corresponds to a given strain-rate, the solution of a strongly nonlinear system of equations is necessary. The basic equations are as follows:

By neglecting elastic distortion, the macroscopic Eulerian strain-rate components are obtained from the crystallographic slips using

$$\dot{\varepsilon}_{ij} = \frac{1}{2} \sum_{f=1}^{nf} \sum_{s=1}^{nsf} (m_{ij}^{s,f} + m_{ji}^{s,f}) \dot{\gamma}^{s,f}, \tag{2}$$

where nsf is the number of slip systems in family f and $m_{ij}^{s,f}$ is the Schmid orientation matrix of slip system s:

$$m_{ij}^{s,f} = \mathbf{b}_i^{s,f} \mathbf{n}_j^{s,f}, \tag{3}$$

with $\mathbf{b}^{s,f}$ and $\mathbf{n}^{s,f}$ being the slip direction and slip plane normal unit vectors, respectively. The total number of families is nf. The resolved shear stress is related to the Cauchy stress tensor $\boldsymbol{\sigma}$ as follows:

$$\tau^{s,f} = \sigma_{ij} m_{ij}^{s,f}, \tag{4}$$

which permits us to write Eq. (2), with the help of Eq. (1), in the form:

$$\dot{\varepsilon}_{ij} = \frac{\dot{\gamma}_0}{2} \sum_{f=1}^{nf} \frac{1}{(\tau_0^f)^{1/m}} \sum_{s=1}^{nsf} \left(m_{ij}^{s,f} + m_{ji}^{s,f}\right)\left(\sigma_{kl} m_{kl}^{s,f}\right) \left|\sigma_{pq} m_{pq}^{s,f}\right|^{\frac{1}{m}-1}. \tag{5}$$

(Unless otherwise stated, summation is implied for the repeated indices throughout this paper.) Only the deviatoric part $\mathbf{S}$ of the stress state $\boldsymbol{\sigma}$ affects the resolved shear stress, so $\boldsymbol{\sigma}$ can replaced by $\mathbf{S}$ in Eq. (5). In order to simplify Eq. (5), 5-component vector quantities are introduced. For this purpose, Lequeu's notation is adopted here (Lequeu et al., 1987):

$$\underline{S} = \left(\frac{(S_{22} - S_{11})}{\sqrt{2}}, \frac{\sqrt{3}}{\sqrt{2}} S_{33}, \sqrt{2} S_{23}, \sqrt{2} S_{31}, \sqrt{2} S_{12}\right), \tag{6}$$

$$\underline{\dot{\varepsilon}} = \left(\frac{(\dot{\varepsilon}_{22} - \dot{\varepsilon}_{11})}{\sqrt{2}}, \frac{\sqrt{3}}{\sqrt{2}} \dot{\varepsilon}_{33}, \sqrt{2} \dot{\varepsilon}_{23}, \sqrt{2} \dot{\varepsilon}_{31}, \sqrt{2} \dot{\varepsilon}_{12}\right), \tag{7}$$

$$\underline{M}^{s,f} = \left(\frac{(m_{22}^{s,f} - m_{11}^{s,f})}{\sqrt{2}}, \frac{\sqrt{3}}{\sqrt{2}} m_{33}^{s,f}, \frac{(m_{23}^{s,f} + m_{32}^{s,f})}{\sqrt{2}}, \frac{(m_{31}^{s,f} + m_{13}^{s,f})}{\sqrt{2}}, \frac{(m_{12}^{s,f} + m_{21}^{s,f})}{\sqrt{2}}\right). \tag{8}$$

With the above definitions, Eq. (5) can be written as:

$$\dot{\varepsilon}_i = \dot{\gamma}_0 \sum_{f=1}^{nf} \frac{1}{(\tau_0^f)^{1/m}} \sum_{s=1}^{nsf} M_i^{s,f} (S_k M_k^{s,f}) |S_l M_l^{s,f}|^{\frac{1}{m}-1}. \tag{9}$$

This relation represents five equations for the five independent components of the strain-rate vector $\dot{\varepsilon}$. The unknowns are the components of the deviatoric stress vector $\mathbf{S}$. Eq. (9) is strongly nonlinear because the m value is usually small for typical applications. It is commonly solved in an iterative way with the help of the Newton–Raphson scheme. Such an iteration scheme requires a good initial guess. For this purpose, the solution from the linear case $m = 1$ can be employed. This case of linear viscous slip is treated in the second part of the paper. This case is also important in creep. Dislocation creep can be well described by Eq. (1) when $m = 1$ (Vreeland, 1968):

$$\tau^{s,f} = \tau_0^f \frac{\dot{\gamma}^{s,f}}{\dot{\gamma}_0}. \tag{10}$$

Superplastic deformation also corresponds to large m values, approaching even the value of 1.0. Although superplastic deformation is believed to be achieved by grain boundary sliding in combination with dislocation glide, the former mechanism, being strongly dependent on diffusion, naturally leads to a high amount of strain-rate sensitivity. Grain boundary sliding is also believed to be the cause of the randomization of texture, as observed during superplastic deformation. However, it is possible that the role of grain boundary sliding is over-emphasized in some cases. In such cases, the high value of m would indeed be due to the behaviour of dislocations, and Eq. (10) applies; this would also explain the slow or lack of development of deformation textures, as high values of m correspond to a low or zero plastic spin.

Note that the above constitutive equation corresponds to a very special case of crystal viscoplasticity. Situations when it can be applied correspond to high temperature deformation or creep. In most practical applications, the strain-rate sensitivity index m is very small; in certain cases it may even be negligible from the engineering point of view. However, the limiting case $m = 1$ of viscoplasticity could provide useful insight for understand-

ing certain trends of crystal behaviour. Eq. (10) is also useful as an initial numerical guess for solving the highly nonlinear system of equations in viscoplasticity when $m \ll 1$.

The subject of the second part of the paper is to show that, for cubic and hexagonal crystal systems, the solution for the linear viscous case is completely analytic. Not even a linear system of equations has to be solved (Eq. (9) with $m = 1$) to obtain the stress response of the material for a given strain-rate. The equi-potential surfaces are also examined both in stress and in strain-rate spaces.

Finally, the lattice rotations are examined for the linear viscous case. Although the plastic spin has already been shown to be zero for fcc crystal structures when $m = 1$ (Tóth et al., 1988), the case for hexagonal crystal structures has not yet been examined.

2. The stress and strain-rate potential functions

As there is no threshold yield stress for strain-rate sensitive slip of the type described by Eq. (1), a "yield surface" in the classical sense does not exist. However, the behaviour of the crystal can still be visualized with the help of a stress potential function. Such an analysis has been carried out for fcc single crystals by Tóth et al. (1988). The shapes of the yield potentials give direct information about the plastic anisotropy of the crystal. There also exists a dual function to the stress potential, which is referred to as the strain-rate potential function (Van Houtte, 2002). The latter is very useful when known analytically as it permits us to readily obtain the stress state for any given applied strain-rate. Such an analysis has not yet been carried out for hcp structures.

An equi-potential is defined such that the plastic power $\dot{W}$ is constant along its surface; i.e.,

$$\dot{W} = S_i \dot{\varepsilon}_i = \sum_{f=1}^{nf} \sum_{s=1}^{nsf} \tau^{s,f} \dot{\gamma}^{s,f} = C. \tag{11}$$

With the help of Eq. (1), $\dot{W}$ becomes:

$$\dot{W} = \sum_{f=1}^{nf} \frac{\dot{\gamma}_0}{(\tau_0^f)^{1/m}} \sum_{s=1}^{nsf} |M_i^{s,f} S_i|^{\frac{1}{m}+1} = C. \tag{12}$$

The stress potential function $f(\underline{S})$ is defined so that the plastic strain-rate (in vector form) is normal to it:

$$\dot{\varepsilon}_i = \frac{\partial f(\underline{S})}{\partial S_i}. \tag{13}$$

Under this condition, $f(\underline{S})$ can be expressed as:

$$f(\underline{S}) = \frac{m}{m+1} \sum_{f=1}^{nf} \frac{\dot{\gamma}_0}{(\tau_0^f)^{1/m}} \sum_{s=1}^{nsf} |M_i^{s,f} S_i|^{\frac{1}{m}+1} = C. \tag{14}$$

Similarly, the strain-rate potential function $h(\underline{\dot{\varepsilon}})$ is such that the stress state (in vector form) is perpendicular to it:

$$S_i = \frac{\partial h(\underline{\dot{\varepsilon}})}{\partial \dot{\varepsilon}_i}. \tag{15}$$

Unfortunately, an analytic form for $h(\underline{\dot{\varepsilon}})$ cannot be given (except for $m = 1$, see below), although it would be very useful to obtain the stress state from the imposed strain-rate without any numerical iteration. Nevertheless, the equi-potential surfaces of $h(\underline{\dot{\varepsilon}})$ can be plotted numerically as the strain-rate can always be computed from Eq. (9) from the stress state corresponding to the stress-potential surface. The two functions $f(\underline{S})$ and $h(\underline{\dot{\varepsilon}})$ are dual potentials. The potential $h(\underline{\dot{\varepsilon}})$ has been examined by Fortunier (1989) for the cubic structure in rate-independent slip, when the Schmid law can be used. In this work $h(\underline{\dot{\varepsilon}})$ is computed numerically for different m values. The limiting case $m = 0$ can be approximated by using very low m values.

The equi-potentials were calculated in the crystal reference system for hexagonal crystal structures ($c/a = 1.624$, magnesium) with the following available slip system families: basal, prismatic, pyramidal $\langle a\rangle$, pyramidal $\langle c + a\rangle/A$ and $\langle c + a\rangle/B$. A series of m values were considered: $m = 1, 0.5, 0.2, 0.1, 0.05$ and 0 for the stress potentials as well as $m = 1, 0.5, 0.2, 0.1, 0.05, 0.005$ for the strain-rate potentials. The constant C in the expression of $f(\underline{S})$ (Eq. (14)) was chosen as: $C = \tau_0^{\text{basal}}\dot{\gamma}_0 m/(m+1)$. Here $\tau_0^{\text{basal}}\dot{\gamma}_0$ is a plastic power that would correspond to the power in single slip within one basal slip system when the resolved shear stress is equal to the reference strength τ_0^{basal} and the slip rate is $\dot{\gamma}_0 = 1.0\ \text{s}^{-1}$. All obtained stress components are expressed in units of τ_0^{basal}. The Cartesian reference system was defined as follows: $x_1 \| [1\,0\,\bar{1}\,0], x_2 \| [\bar{1}\,2\,\bar{1}\,0], x_3 \| [0\,0\,0\,1]$.

Figs. 1 and 2 show the stress and strain-rate equi-potentials for two different relative strengths of the available five slip system families; in Fig. 1, all slip systems are considered to have the same strength as the basal slip; in Fig. 2, the following relative strengths were used: $\tau_0^{\text{prism.}} = \tau_0^{\text{pyr.}\langle a\rangle} = 8\tau_0^{\text{basal}}, \tau_0^{\text{pyr.}\langle c+a\rangle/A} = \tau_0^{\text{pyr.}\langle c+a\rangle/B} = 6\tau_0^{\text{basal}}$. (A complete list of the slip systems can be found in Table 1.) The stress potentials for the limiting $m = 0$ case were plotted using the Schmid criterion. They are analogous to the Bishop and Hill surface known for fcc materials. It has already been shown in Tóth et al. (1988) that the stress potential surfaces converge to the Bishop and Hill yield surface as $m \to 0$ in the fcc crystal structure. That result can also be readily transposed to hcp crystal structures in viscoplastic slip.

As can be seen in Figs. 1 and 2, the shapes of the equi-potential surfaces become more and more rounded as the m value is increased and, as expected, sharp vertices appear in the limiting case of rate-independent behaviour ($m = 0$). For this limiting case, the active slip system families are indicated along the stress potential surfaces in Figs. 1 and 2. Because of the reduced symmetries in hcp structures as compared to the fcc case, the potential functions also display fewer symmetries. This is why not all the potentials exhibit a mirror symmetry with respect to the stress coordinate axes. The different sections differ also in the active slip system families. For example, only basal slip is active in the $S_4 - S_3$ section, while in the $S_2 - S_1$ section, basal slip is eliminated. This effect is sharply affected by the choice of the relative strengths of the slip systems: when non-basal slips are much more difficult (Fig. 2), prismatic slip is completely eliminated in the sections presented. This effect depends, of course, on the hcp lattice parameter, too; when the c/a ratio is increased, the pyramidal type systems become less inclined to the c-axis which leads to reduced resolved shear stress, for example, for a tensile loading parallel to the c-axis. By varying the c/a ratio, the $M_i^{s,f}$ values change. Table 1 shows the $M_i^{s,f}$ values for each slip system as a function of the c/a parameter (named c_a). The stress levels – that is, the sizes of the potentials – also depend on the relative strengths of the slip system families (except the

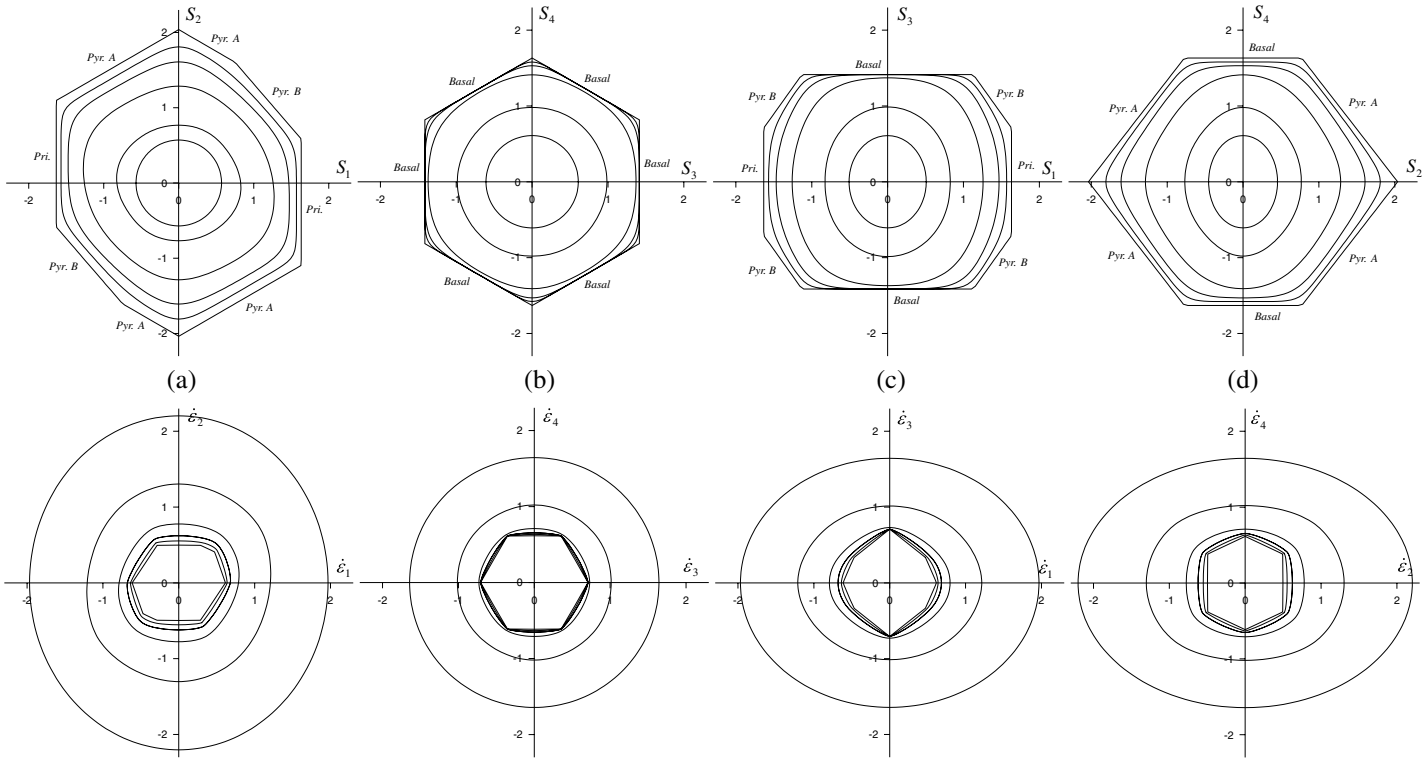

Fig. 1. Stress $f(S)$ (top) and strain-rate $h(\dot{\varepsilon})$ (bottom) equi-potentials in hexagonal crystal structures ($c/a = 1.624$, magnesium) for different sections in Lequeu space, for different values of m (for $f(S)$: $m = 1, 0.5, 0.2, 0.1, 0.05, 0$, for $h(\dot{\varepsilon})$: $m = 1, 0.5, 0.2, 0.1, 0.05, 0.005$). For $f(S)$, the smallest surface corresponds to $m = 1$, while for $h(\dot{\varepsilon})$, the order is opposite. The relative strengths of all slip system families are equal. Stress values are in units of the slip system strength. Strain-rate values are in s^{-1}.

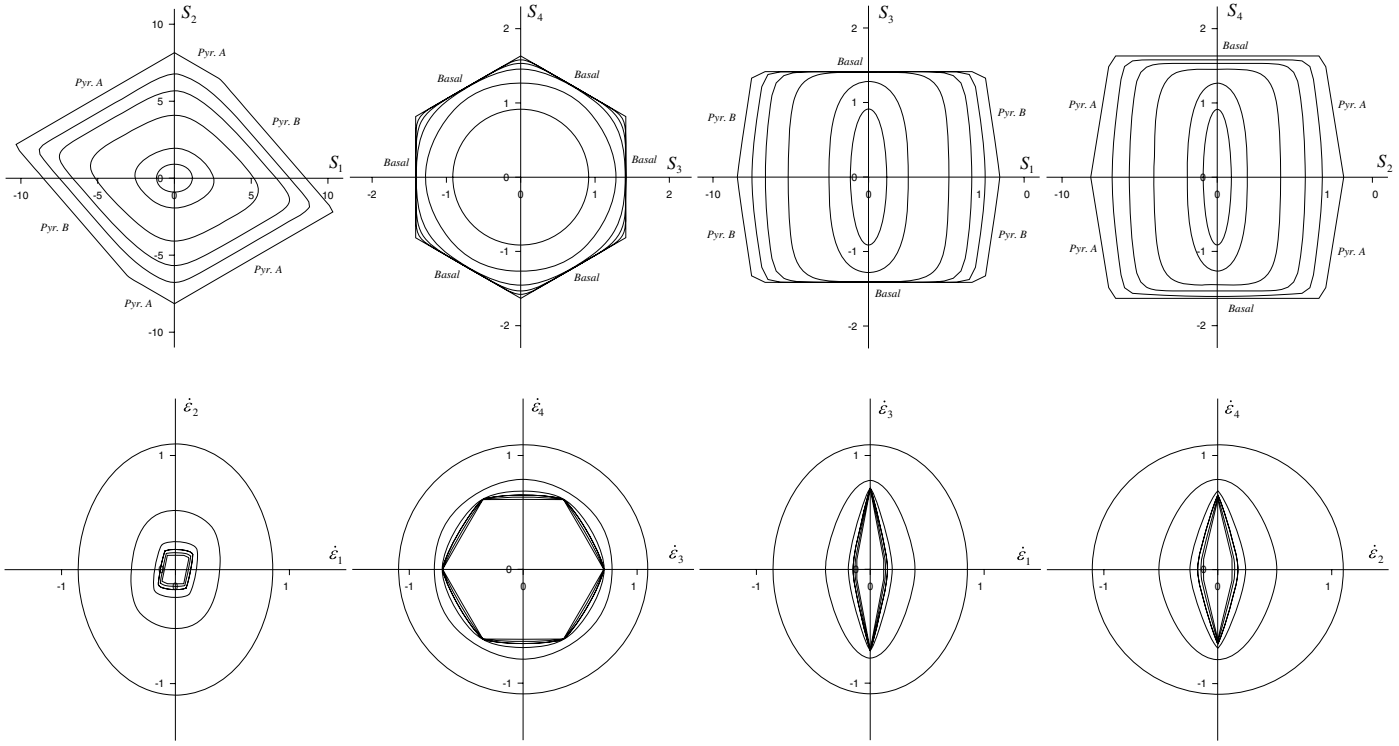

Fig. 2. Equi-potentials $f(S)$ (top) and $h(\dot{\varepsilon})$ (bottom) in hexagonal structures (magnesium $c/a = 1.624$) for different sections in Lequeu space, for different values of m (for $f(S)$: $m = 1, 0.5, 0.2, 0.1, 0.05, 0$, for $h(\dot{\varepsilon})$, $m = 1, 0.5, 0.2, 0.1, 0.05, 0.005$). For $f(S)$, the smallest surface corresponds to $m = 1$, while for $h(\dot{\varepsilon})$, the order is opposite. The relative strengths of the slip systems are: $\tau_0^{\text{prism.}} = \tau_0^{\text{pyr.}\langle a\rangle} = 8\tau_0^{\text{basal}}$, $\tau_0^{\text{pyr.}\langle c+a\rangle/A} = \tau_0^{\text{pyr.}\langle c+a\rangle/B} = 4\tau_0^{\text{basal}}$. Stress values are normalized with respect to the reference strength of basal slip. Strain-rate values are in s^{-1}.

Table 1
Schmid tensors $M_i^{s,f}$ for hexagonal structure in five dimensions

Family f	Systems s	$M_1^{s,f}$	$M_2^{s,f}$	$M_3^{s,f}$	$M_4^{s,f}$	$M_5^{s,f}$	Division factor
Basal	$(0001)[1\bar{2}10]$	0	0	-1	0	0	$\sqrt{2}$
	$(0001)[2\bar{1}\bar{1}0]$	0	0	$-1/2$	$\sqrt{3}/2$	0	
	$(0001)[11\bar{2}0]$	0	0	$1/2$	$\sqrt{3}/2$	0	
Prismatic	$(10\bar{1}0)[\bar{1}2\bar{1}0]$	0	0	0	0	1	$\sqrt{2}$
	$(1\bar{1}00)[11\bar{2}0]$	$-\sqrt{3}/2$	0	0	0	$-1/2$	
	$(0\bar{1}10)[2\bar{1}\bar{1}0]$	$\sqrt{3}/2$	0	0	0	$-1/2$	
Pyramidal $\langle a\rangle$	$(10\bar{1}1)[\bar{1}2\bar{1}0]$	0	0	$\sqrt{3}/c_a$	0	2	$\sqrt{2}\sqrt{4+3/c_a^2}$
	$(1\bar{1}01)[11\bar{2}0]$	$-\sqrt{3}$	0	$\sqrt{3}/2c_a$	$3/2c_a$	-1	
	$(0\bar{1}11)[2\bar{1}\bar{1}0]$	$\sqrt{3}$	0	$-\sqrt{3}/2c_a$	$3/2c_a$	-1	
	$(\bar{1}011)[1\bar{2}10]$	0	0	$-\sqrt{3}/c_a$	0	2	
	$(\bar{1}101)[\bar{1}\bar{1}20]$	$-\sqrt{3}$	0	$-\sqrt{3}/2c_a$	$-3/2c_a$	-1	
	$(01\bar{1}1)[\bar{2}110]$	$\sqrt{3}$	0	$\sqrt{3}/2c_a$	$-3/2c_a$	-1	
Pyramidal $\langle c+a\rangle/A$	$(10\bar{1}1)[2\bar{1}\bar{1}\bar{3}]$	$-\sqrt{3}$	-3	$-\sqrt{3}/2c_a$	$-(4c_a^2-3)/2c_a$	-1	$\sqrt{2}\sqrt{4+3/c_a^2}$
	$(10\bar{1}1)[11\bar{2}\bar{3}]$	$-\sqrt{3}$	-3	$\sqrt{3}/2c_a$	$-(4c_a^2-3)/2c_a$	1	$\sqrt{1+c_a^2}$
	$(01\bar{1}1)[11\bar{2}\bar{3}]$	0	-3	$-\sqrt{3}(2c_a^2-1)/2c_a$	$-(2c_a^2-3)/2c_a$	2	
	$(01\bar{1}1)[\bar{1}2\bar{1}\bar{3}]$	$\sqrt{3}$	-3	$-\sqrt{3}(c_a^2-1)/c_a$	$-c_a$	1	
	$(\bar{1}101)[\bar{1}2\bar{1}\bar{3}]$	$\sqrt{3}$	-3	$-\sqrt{3}(c_a^2-1)/c_a$	c_a	-1	
	$(\bar{1}101)[\bar{2}11\bar{3}]$	0	-3	$-\sqrt{3}(2c_a^2-1)/2c_a$	$(2c_a^2-3)/2c_a$	-2	
	$(\bar{1}011)[\bar{2}11\bar{3}]$	$\sqrt{3}$	-3	$\sqrt{3}/2c_a$	$(4c_a^2-3)/2c_a$	-1	
	$(\bar{1}011)[\bar{1}\bar{1}2\bar{3}]$	$-\sqrt{3}$	-3	$-\sqrt{3}/2c_a$	$(4c_a^2-3)/2c_a$	1	
	$(0\bar{1}11)[\bar{1}\bar{1}2\bar{3}]$	0	-3	$\sqrt{3}(2c_a^2-1)/2c_a$	$(2c_a^2-3)/2c_a$	2	
	$(0\bar{1}11)[1\bar{2}1\bar{3}]$	$\sqrt{3}$	-3	$\sqrt{3}(c_a^2-1)/c_a$	c_a	1	
	$(1\bar{1}01)[\bar{1}\bar{2}1\bar{3}]$	$\sqrt{3}$	-3	$\sqrt{3}(c_a^2-1)/c_a$	$-c_a$	-1	
	$(1\bar{1}01)[2\bar{1}\bar{1}\bar{3}]$	0	-3	$\sqrt{3}(2c_a^2-1)/2c_a$	$-(2c_a^2-3)/2c_a$	-2	
Pyramidal $\langle c+a\rangle/B$	$(2\bar{1}\bar{1}2)[\bar{2}4\bar{2}3]$	-1	$\sqrt{3}$	$-(c_a^2-4)/2c_a$	$c_a^2\sqrt{3}/2$	$\sqrt{3}$	$\sqrt{2}\sqrt{1+1/c_a^2}$
	$(2\bar{1}\bar{1}2)[\bar{2}\bar{2}43]$	2	$\sqrt{3}$	$-(2+c_a^2)/2c_a$	$(c_a^2-2)\sqrt{3}/2c_a$	0	$\sqrt{4+c_a^2}$
	$(1\bar{2}12)[22\bar{4}3]$	-1	$\sqrt{3}$	$-(c_a^2-1)/c_a$	$\sqrt{3}/c_a$	$-\sqrt{3}$	
	$(1\bar{2}12)[\bar{4}223]$	-1	$\sqrt{3}$	$-(c_a^2-1)/c_a$	$-\sqrt{3}/c_a$	$\sqrt{3}$	
	$(\bar{1}\bar{1}22)[4\bar{2}\bar{2}3]$	2	$\sqrt{3}$	$-(2+c_a^2)/2c_a$	$-(c_a^2-2)\sqrt{3}/2c_a$	0	
	$(\bar{1}\bar{1}22)[\bar{2}4\bar{2}3]$	-1	$\sqrt{3}$	$-(c_a^2-4)/2c_a$	$-c_a^2\sqrt{3}/2$	$-\sqrt{3}$	
	$(\bar{2}112)[2\bar{4}\bar{2}3]$	-1	$\sqrt{3}$	$(c_a^2-4)/2c_a$	$-c_a^2\sqrt{3}/2$	$\sqrt{3}$	
	$(\bar{2}112)[22\bar{4}3]$	2	$\sqrt{3}$	$(2+c_a^2)/2c_a$	$-(c_a^2-2)\sqrt{3}/2c_a$	0	
	$(\bar{1}2\bar{1}2)[\bar{2}\bar{2}43]$	-1	$\sqrt{3}$	$(c_a^2-1)/2c_a$	$-\sqrt{3}/c_a$	$-\sqrt{3}$	
	$(\bar{1}2\bar{1}2)[\bar{4}\bar{2}\bar{2}3]$	-1	$\sqrt{3}$	$(c_a^2-1)/c_a$	$\sqrt{3}/c_a$	$\sqrt{3}$	
	$(11\bar{2}2)[\bar{4}223]$	2	$\sqrt{3}$	$(2+c_a^2)/2c_a$	$(c_a^2-2)\sqrt{3}/2c_a$	0	
	$(11\bar{2}2)[2\bar{4}\bar{2}3]$	-1	$\sqrt{3}$	$(c_a^2-4)/2c_a$	$c_a^2\sqrt{3}/2$	$-\sqrt{3}$	

$S_4 - S_3$ section where only basal slip is active). This is why different scales are used in Fig. 2, depending on the section considered.

Concerning the strain-rate potentials, their shapes and sizes are reversed with respect to the stress potential surfaces. The surfaces corresponding to the lower m values are now the inner ones. This reversal in the relative size is due to the fact that the plastic power is the same along all surfaces, so when the stress level is high, the strain-rate must be low. The differences in the shapes of the strain-rate potentials with respect to the stress potential surfaces are due to the duality of these surfaces. As discussed by Hill (1987) for the rate insensitive case, the vertices of the stress potentials correspond to the outer directions (or poles) of the hyperplanes composing the strain-rate potentials (and inversely). Fortunier (1989)

presented the strain-rate potential surfaces dual to the Bishop and Hill surfaces when $m = 0$ for the fcc structure. Although the procedure of Fortunier could also be established for the hcp case, in the present paper the $m = 0$ case was approximated by using a very small strain-rate sensitivity value: $m = 0.005$ in Figs. 1 and 2.

Not all the sections shown in Figs. 1 and 2 are closed. A closed surface means that the strain-rate associated with any admissible stress state in the given section is also located in the same section (Canova et al., 1985). Table 2 shows the results for all sections (from one to four dimensions) obtained for the present hcp case in comparison to the cubic structure. It can be seen in Table 2 that when in the cubic system a sub-space is not closed, it is also not closed in the hexagonal case. Inversely, however, when a sub-space in the cubic case is closed, it can be not closed in the hexagonal case. This is again the consequence of the larger degree of anisotropy of hexagonal structures with respect to the cubic case.

Table 2
Closed (c) or not closed (nc) sub-spaces for hexagonal and cubic structures in five dimensions

Sub-space of imposed stress state					Sub-space of corresponding strain-rate state					Closed (c) or not closed (nc) sub-spaces	
S_1	S_2	S_3	S_4	S_5	$\dot{\varepsilon}_1$	$\dot{\varepsilon}_2$	$\dot{\varepsilon}_3$	$\dot{\varepsilon}_4$	$\dot{\varepsilon}_5$	hcp	cubic
X	0	0	0	0	X	0	0	0	0	c	c
0	X	0	0	0	X	X	0	0	0	nc	c
0	0	X	0	0	0	0	X	0	0	c	c
0	0	0	X	0	0	0	X	X	0	nc	c
0	0	0	0	X	0	0	0	0	X	c	c
X	X	0	0	0	X	X	0	0	0	c	c
X	0	X	0	0	X	X	X	0	0	nc	nc
X	0	0	X	0	X	X	0	X	0	nc	nc
X	0	0	0	X	X	0	0	0	X	c	c
0	X	X	0	0	X	X	X	0	0	nc	nc
0	X	0	X	0	X	X	0	X	0	nc	nc
0	X	0	0	X	X	X	0	0	X	nc	c
0	0	X	X	0	0	0	X	X	0	c	c
0	0	X	0	X	0	0	X	0	X	c	c
0	0	0	X	X	X	X	X	X	X	nc	c
X	X	X	0	0	X	X	X	0	0	c	c
X	X	0	X	0	X	X	0	X	0	c	c
X	X	0	0	X	X	X	0	0	X	c	c
X	0	X	X	0	X	X	X	X	X	nc	nc
X	0	X	0	X	X	X	X	X	X	nc	nc
X	0	0	X	X	X	X	X	X	X	nc	nc
0	X	X	X	0	X	X	X	X	X	nc	nc
0	X	X	0	X	X	X	X	X	X	nc	nc
0	X	0	X	X	X	X	X	X	X	nc	nc
0	0	X	X	X	X	X	X	X	X	nc	c
X	X	X	X	0	X	X	X	X	X	nc	c
X	X	X	0	X	X	X	X	X	X	nc	c
X	X	0	X	X	X	X	X	X	X	nc	c
X	0	X	X	X	X	X	X	X	X	nc	nc
0	X	X	X	X	X	X	X	X	X	nc	nc

3. The case of linear viscous slip; $m = 1$

For the case of linear viscous slip, $m = 1$, an analytic relation between the strain-rate state and deviatoric stress state can be obtained. Using vector quantities, Eq. (2) becomes:

$$\dot{\varepsilon}_i = \sum_{f=1}^{nf} \sum_{s=1}^{nsf} M_i^{s,f} \dot{\gamma}^{s,f}. \tag{16}$$

Eqs. (4) and (10) lead to:

$$\dot{\gamma}^{s,f} = \frac{\dot{\gamma}_0}{\tau_0^f} M_i^{s,f} S_i. \tag{17}$$

Finally, $\dot{\varepsilon}_i$ can be expressed as follows:

$$\dot{\varepsilon}_i = \dot{\gamma}_0 \sum_{f=1}^{nf} \sum_{s=1}^{nsf} \left(\frac{1}{\tau_0^f}\right) M_i^{s,f} M_j^{s,f} S_j. \tag{18}$$

This relation can be re-written as:

$$\dot{\varepsilon}_i = \dot{\gamma}_0 S_j \sum_{f=1}^{nf} \frac{1}{\tau_0^f} \sum_{s=1}^{nsf} M_i^{s,f} M_j^{s,f}. \tag{19}$$

By defining

$$H_{ij}^f = \sum_{s=1}^{nsf} M_i^{s,f} M_j^{s,f}, \tag{20}$$

Eq. (19) becomes:

$$\dot{\varepsilon}_i = \dot{\gamma}_0 S_j \sum_{f=1}^{nf} \frac{1}{\tau_0^f} H_{ij}^f. \tag{21}$$

This relation can still be simplified by introducing the general notation:

$$H_{ij} = \sum_{f=1}^{nf} \frac{1}{\tau_0^f} H_{ij}^f, \tag{22}$$

which allows us to express Eq. (21) as follows:

$$\dot{\varepsilon}_i = \dot{\gamma}_0 H_{ij} S_j. \tag{23}$$

The H_{ij}^f matrix has a special property in the crystal reference system: *it is diagonal* for all slip system families of bcc, fcc and even for hcp crystal structures. Consequently, H_{ij} is also diagonal. This property, unfortunately, is lost when the $m_{ij}^{s,f}$ quantities are expressed in any other reference system. Because of the diagonal nature of H_{ij}^f, the stress state can be readily obtained from Eq. (23) as follows:

$$S_i = \frac{\dot{\varepsilon}_i}{\dot{\gamma}_0 H_{(ii)}}, \tag{24}$$

where the parenthesis (ii) denotes *no* summation on i.

The values of the diagonal components of H_{ij}^{f} are shown in Table 3 for bcc, fcc and hcp crystal structures. In the example shown, all τ_0^f values were taken to be 1 MPa.

The result expressed by Eq. (24) is very useful in rate-sensitive crystal plasticity calculations and allows the stress response of the crystal to be immediately obtained for any imposed strain-rate in an analytic way (i.e., without solving any equation). Note, however, that this is only valid for linear viscous plastic slip of a crystal; i.e., when $m = 1$.

Now the stress and strain-rate potentials can be examined for the restricted case of linear viscous slip. Using Eq. (23), the condition given by Eq. (11) becomes:

$$\dot{W} = \frac{1}{\dot{\gamma}_0} \sum_{i=1}^{5} \frac{(\dot{\varepsilon}_i)^2}{H_{(ii)}} = C. \tag{25}$$

Now the strain-rate potential function $h(\dot{\boldsymbol{\varepsilon}})$ will be determined. A normal vector to its surface should give the deviatoric stress, i.e.,

$$S_i = \lambda \frac{\partial h(\dot{\boldsymbol{\varepsilon}})}{\partial \dot{\varepsilon}_i}. \tag{26}$$

where λ is a positive scalar factor. Using Eq. (25), $h(\dot{\varepsilon})$ can be readily obtained:

$$h(\dot{\varepsilon}) = \frac{1}{2\dot{\gamma}_0} \sum_{i=1}^{5} \frac{(\dot{\varepsilon}_i)^2}{H_{(ii)}}. \tag{27}$$

The value of λ is 0.5 (obtained from Eqs. (24) and (26)). It can be readily verified that by substituting $h(\dot{\boldsymbol{\varepsilon}})$ in Eq. (26) we recover Eq. (24).

The stress potential surface can be obtained from Eq. (27) using Eq. (24):

$$f(S) = \sum_{i=1}^{5} (S_i)^2 H_{(ii)}. \tag{28}$$

It is obvious from the expression of the equi-potentials that they are not defined if one of the $H_{(ii)}$ values is zero. This does not happen in fcc and bcc structures; it happens, however, in hcp crystal systems when the basal, prismatic or pyramidal $\langle a \rangle$ slip systems are considered alone (see Table 3). This also follows from the well-known deficiency of strain accommodation for hcp structures; i.e., that these slip systems alone are not sufficient to

Table 3
H_{ii}^{f} values in fcc, bcc and hcp (magnesium, $c/a = 1.624$) structures

Families		H_{11}	H_{22}	H_{33}	H_{44}	H_{55}
fcc	$\{111\}\langle 110\rangle$	2	2	2/3	2/3	2/3
bcc	$\{110\}\langle 110\rangle$	2	2	2/3	2/3	2/3
	$\{112\}\langle 111\rangle$	2	2	2/3	2/3	2/3
	$\{123\}\langle 111\rangle$	4	4	4/3	4/3	4/3
hcp	Basal – $\{0001\}\langle 11\bar{2}0\rangle$	0	0	0.75	0.75	0
	Prismatic – $\{10\bar{1}0\}\langle \bar{1}1\bar{2}0\rangle$	0.75	0	0	0	0.75
	Pyr.$\langle a\rangle$ – $\{10\bar{1}1\}\langle \bar{1}2\bar{1}0\rangle$	1.17	0	0.33	0.33	1.17
	Pyr.$\langle c+a\rangle/A$ – $\{01\bar{1}1\}\langle 11\bar{2}\bar{3}\rangle$	0.64	2.89	0.91	0.91	0.64
	Pyr.$\langle c+a\rangle/B$ – $\{11\bar{2}2\}\langle 2\bar{4}23\rangle$	1.31	1.97	0.71	0.71	1.31

permit an arbitrary deformation of the crystal without adding to them the pyramidal slip system family. The pyramidal $\langle c+a\rangle/A$ and pyramidal $\langle c+a\rangle/B$ slip system families, however, can accommodate any imposed deformation.

For the shape and size variations of the strain-rate $h(\dot{\boldsymbol{\varepsilon}})$ and stress equi-potentials $f(S)$ for the hexagonal crystal structure ($c/a = 1.624$, magnesium) in the present linear case, see Figs. 1 and 2.

4. Plastic spin

Over the years, there has been considerable interest in the concept of plastic spin in the plasticity community. Even in phenomenological constitutive modelling the plastic spin has been employed to describe the evolution of anisotropy (see, for example, Dafalias and Rashid, 1989; Van der Giessen et al., 1992; Bunge and Nielsen, 1997; Song and Voyiadjis, 2002; Gurtin and Anand, 2005). In crystal plasticity, the plastic spin is an important element in the calculation of the lattice spin (see, for example, Havner, 1981; Tóth et al., 1988, 1990; Aravas and Aifantis, 1991; Dafalias, 1998; Van Houtte, 2002).

It is necessary to distinguish among three types of rotation when the lattice spin of a crystal due to plastic slip is calculated (assuming that elastic distortions are neglected). They are:

$\underline{\underline{\beta}}$, the *material spin*, which is the skew-symmetric part of the velocity gradient $\boldsymbol{L}$ relative to the fixed reference system and given by

$$\beta_{ij} = \frac{\boldsymbol{L}_{ij} - \boldsymbol{L}_{ji}}{2}; \tag{29}$$

$\underline{\underline{\omega}}$, the *plastic spin*, which is the skew-symmetric part of the velocity gradient corresponding to the plastic slip alone; with respect to the fixed reference system it is given by (Havner, 1981, 1984):

$$\omega_{ij} = \sum_{f=1}^{nf}\sum_{s=1}^{nsf}\frac{m_{ij}^{s,f} - m_{ji}^{s,f}}{2}\dot{\gamma}^{s,f}; \tag{30}$$

$\underline{\underline{\Omega}}$, the *lattice spin*, which is the rate of rotation of the crystallographic directions with respect to the fixed reference system.

The following relation exists between these quantities (Havner, 1972):

$$\underline{\underline{\omega}} = \underline{\underline{\beta}} - \underline{\underline{\Omega}}. \tag{31}$$

In the following, the plastic spin will be evaluated in detail. By using the constitutive law Eq. (1) together with Eq. (4), Eq. (30) becomes:

$$\omega_{ij} = \frac{\dot{\gamma}_0}{2}\sum_{f=1}^{nf}\frac{1}{(\tau_0^f)^{1/m}}\sum_{s=1}^{nsf}(m_{ij}^{s,f} - m_{ji}^{s,f})m_{kl}^{s,f}S_{kl}\left|m_{pq}^{s,f}S_{pq}\right|^{\frac{1}{m}-1}. \tag{32}$$

For $m = 1$ this relation reads:

$$\omega_{ij} = \frac{\dot{\gamma}_0}{2}S_{kl}\sum_{f=1}^{nf}\frac{1}{\tau_0^f}\sum_{s=1}^{nsf}(m_{ij}^{s,f} - m_{ji}^{s,f})m_{kl}^{s,f}. \tag{33}$$

By defining:

$$H^f_{ijkl} = \sum_{s=1}^{nsf} m^{s,f}_{ij} m^{s,f}_{kl}, \tag{34}$$

Eq. (33) becomes:

$$\omega_{ij} = \frac{\dot{\gamma}_0}{2} S_{kl} \sum_{f=1}^{nf} \frac{1}{\tau^f_0} (H^f_{ijkl} - H^f_{jikl}). \tag{35}$$

This relation can be further simplified by introducing the general notation:

$$H_{ijkl} = \sum_{f=1}^{nf} \frac{1}{\tau^f_0} H^f_{ijkl}. \tag{36}$$

As a result, Eq. (35) finally reads:

$$\omega_{ij} = \frac{\dot{\gamma}_0}{2} (H_{ijkl} - H_{jikl}) S_{kl}. \tag{37}$$

The calculation of the H_{ijkl} quantities for all families of slip systems in bcc, fcc and hcp structures gives the following general result (independently of the relative strengths τ^f_0 of the slip system families): for 60 of the 81 cases, $H_{ijkl} = 0$ (for $ij \neq kl$ and $i \neq j$).

Tóth et al. (1988) have shown that the plastic spin is zero for cubic structures when $m = 1$. As a consequence, the lattice rotation rate $\underline{\underline{\Omega}}$ is equal to the material rotation rate $\underline{\underline{\beta}}$. In tension, compression or rolling, the material rotation rate is zero, so the lattice rotation will also vanish. Consequently, there is no evolution of the crystallographic texture in cubic polycrystals for these cases. However, the same conclusion is not valid for the hcp crystal structures. It has been found using Eq. (37) that only rotations around the c-axis vanish ($\omega_{12} = 0$). The other two components of the rotation vector are generally non-zero; i.e., $\omega_{13} \neq 0$ and $\omega_{23} \neq 0$. The reason for this can be that the only symmetry axis in hcp structures is the c-axis, which is the axis of the ω_{12} component of the plastic spin. By contrast, in cubic structures, there is a symmetry for all three crystal axis, and this can be the reason that all components of the plastic spin rotation ω_{ij} are zero for $m = 1$ in that case.

The consequence of the non-zero plastic spin in hexagonal crystal structures is that textures should develop in hcp polycrystals. Nevertheless, it is important to see to what extent the texture can be altered because of the non-zero plastic spin. For this purpose, simulations of texture developments have been carried out for the case of an hcp polycrystalline magnesium. Simple shear has been selected as a deformation path because large strains can be generally achieved in simple shear using torsion testing. A constant velocity gradient was used:

$$\boldsymbol{L} = \begin{pmatrix} 0 & 1.0\,\mathrm{s}^{-1} & 0 \\ 0 & 0 & 0 \\ 0 & 0 & 0 \end{pmatrix}. \tag{38}$$

The rigid body spin corresponding to this velocity gradient is: $\beta_{12} = 0.5\,\mathrm{s}^{-1}$. One hundred randomly oriented grain orientations have been selected for the initial texture, which was centro-symmetrized with respect to axis z of the coordinate system (the only symmetry that applies to shear testing). The distribution in the form of a (0001) pole figure is depicted in Fig. 3a. The relative strengths of the slip systems were $\tau_0^{\mathrm{prism.}} = \tau_0^{\mathrm{pyr.}\langle a\rangle} = 2\tau_0^{\mathrm{basal}}$ and $\tau_0^{\mathrm{pyr.}\langle c+a\rangle/A} = \tau_0^{\mathrm{pyr.}\langle c+a\rangle/B} = 3\tau_0^{\mathrm{basal}}$ (see Agnew et al., 2005).

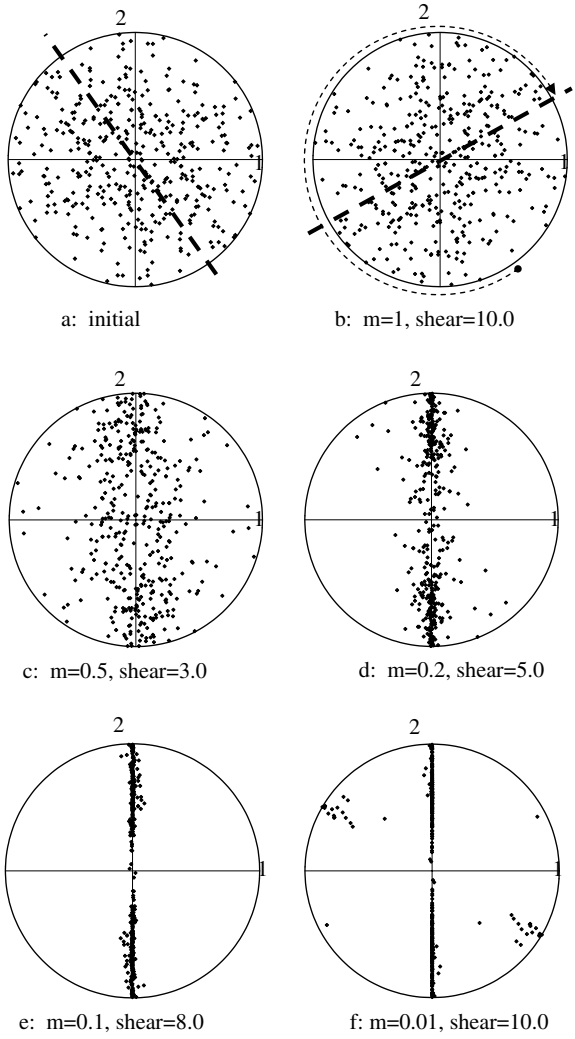

Fig. 3. Simulated texture development during simple shear of polycrystalline magnesium.

The texture development is controlled by the lattice spin $\underline{\underline{\Omega}}$, which is given by Eq. (31); i.e., $\underline{\underline{\Omega}} = \underline{\beta} - \underline{\underline{\omega}}$. The lengths of the lattice and plastic spin vectors are given by:

$$\Omega = \sqrt{\Omega_{32}^2 + \Omega_{13}^2 + \Omega_{12}^2}, \quad \omega = \sqrt{\omega_{32}^2 + \omega_{13}^2 + \omega_{12}^2}. \tag{39}$$

As $\underline{\beta}$ is constant in this example, the evolution of the plastic spin is the decisive factor in the evolution of the texture. As this quantity varies from one crystal to another, an average value $\bar{\omega}$ was calculated to represent the lattice spin of the polycrystal. In Fig. 4, this quantity is plotted as a function of the shear deformation of the simulated polycrystal. As seen in this figure, $\bar{\omega}$ is very low for $m = 1$ (with respect to the value $\beta_{12} = 0.5\ \mathrm{s}^{-1}$); it is only about $0.0285\ \mathrm{s}^{-1}$, and remains practically constant during straining. Consequently, the

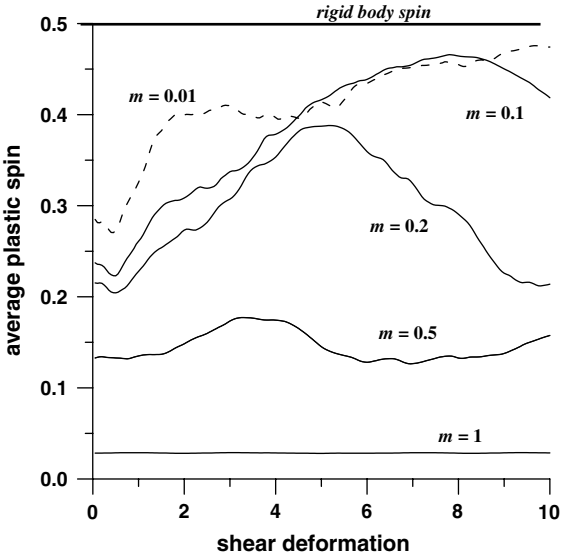

Fig. 4. Evolution of the average plastic spin with shear deformation for hexagonal crystal structured polycrystal (magnesium) for various strain-rate sensitivity index values.

texture development is virtually a simple rotation of the initial texture around the z-axis (the centre of the pole figure) in the clockwise direction. During this large strain simulation (up to a shear strain of 10.0), the expected rotation of the texture can be estimated by an integration of the average lattice spin $\bar{\Omega}$ during straining. This integral leads to the value of 286.5° for the present case. This rotation is indicated in Fig. 3b (with respect to Fig. 3a), which seems to agree well with the overall rotation of the texture. However, the contribution of the plastic spin is very small. For example, the calculated value of the rotation corresponding to a zero value of $\bar{\omega}$ is 285.2°; this is very close to the above value of 286.5° when the plastic spin is included in the computation.

For comparison purposes, simulations have also been carried out for lower m values, down to $m = 0.01$. The obtained average plastic spin increases significantly with m, as seen in Fig. 4. The value of $\bar{\omega}$ also varies as a function of strain, because of the evolution of the crystallographic texture. First it generally increases, then decreases after reaching a local maximum. The textures that correspond to these maximum plastic spin values are displayed in Fig. 3c–f. Only when m is very low can the plastic spin approach the value of the rigid body spin, and only at large strains. At that stage, almost all crystal orientations arrive near stable (ideal) positions in orientation space and the texture becomes very sharp, as seen in Fig. 3f. The effect of the m value on texture development has already been discussed by (Tóth et al., 1988) for the fcc case. Similar findings are valid for the hexagonal crystal structure considered here.

5. Conclusions

The stress and strain-rate potentials have been analysed for hexagonal crystal structures: the effects of viscoplastic slip and the relative strengths of the slip system families

have been highlighted. The case of linear viscous slip in crystal plasticity has also been examined in detail. The stress response of the crystal for a given imposed strain-rate and the plastic spin were determined. The simplicity of the constitutive law and the crystal symmetry allowed the development of direct closed-form analytical relations when $m = 1$. The results of this investigation lead to the following major conclusions for the $m = 1$ case:

1. The stress state corresponding to the imposed strain-rate state can be obtained from a direct linear relation in the crystal reference system.
2. Contrary to the case of cubic crystals, the plastic spin is not zero in hexagonal crystal structures. Nevertheless, its value is very low with respect to the imposed rigid body spin.

Acknowledgements

The authors are thankful to a reviewer for his careful examination and useful comments made on a previous version of this paper. This work was partially funded by the Natural Sciences and Engineering Research Council of Canada (NSERC). K.W.N. is Canada Research Chair in Advanced Engineered Material Systems and the support of this program is gratefully acknowledged.

References

Agnew, S.R., Mehrotra, P., Lillo, T.M., Stoica, G.M., Liaw, P.K., 2005. Texture evolution of five wrought magnesium alloys during route A equal channel angular extrusion: Experiments and simulations. Acta Materialia 53, 3135–3146.

Aravas, N., Aifantis, E.C., 1991. On the geometry of slip and spin in finite plastic deformation. International Journal of Plasticity 7, 141–160.

Asaro, R.J., Needleman, A., 1985. Texture development and strain hardening in rate dependent polycrystals. Acta Metallurgica 33, 923–953.

Bishop, J.F.W., Hill, R., 1951. A theory of the plastic distortion of a polycrystalline aggregate under combined stresses. Philosophical Magazine 42, 414–427.

Bunge, H.J., Nielsen, I., 1997. Experimental determination of plastic spin in polycrystalline materials. International Journal of Plasticity 13, 435–446.

Canova, G.R., Kocks, U.F., Tomé, C.N., Jonas, J.J., 1985. The yield surface of textured polycrystals. Journal of the Mechanics and Physics of Solids 33, 371–397.

Dafalias, Y.F., 1998. Plastic spin: necessity or redundancy. International Journal of Plasticity 14, 909–931.

Dafalias, Y.F., Rashid, M.M., 1989. The effect of plastic spin on anisotropic material behavior. International Journal of Plasticity 5, 227–246.

Fortunier, R., 1989. Dual potentials and extremum work principles in single crystal plasticity. Journal of the Mechanics and Physics of Solids 37 (6), 779–790.

Gurtin, M.E., Anand, L., 2005. The decomposition $F = F^{e}F^{p}$, material symmetry, and plastic irrotationality for solids that are isotropic-viscoplastic or amorphous. International Journal of Plasticity 21, 1686–1719.

Havner, K.S., 1972. On Hill's stress rate in the continuum mechanics of polycrystals. Acta Mechanica 14, 183–187.

Havner, K.S., 1981. A theoretical analysis of finitely deforming f.c.c. crystals in the sixfold symmetry position. Proceedings of the Royal Society of London A378, 329–349.

Havner, K.S., 1984. First- and second-order analysis of axially loaded crystals in n-fold symmetry. Philosophical Transactions of the Royal Society of London A 311, 469–493.

Hill, R., 1987. Constitutive dual potentials in classical plasticity. Journal of the Mechanics and Physics of Solids 35, 23–33.

Hutchinson, J.W., 1976. Bounds and self-consistent estimates for creep of polycrystalline materials. Proceedings of the Royal Society of London A 348, 101–127.

Lequeu, P., Gilormini, P., Montheillet, F., Bacroix, B., Jonas, J.J., 1987. Yield surfaces for textured polycrystals – I. Crystallographic approach. Acta Metallurgica 35 (2), 439–451.

Neale, K.W., Tóth, L.S., Jonas, J.J., 1990. Large strain shear and torsion of rate-sensitive FCC polycrystals. International Journal of Plasticity 6, 45–61.

Song, C.R., Voyiadjis, G.Z., 2002. Microstructure consideration with plastic spin and multiple back-stresses for large strain problems in soils. International Journal of Plasticity 18, 1271–1289.

Tóth, L.S., Gilormini, P., Jonas, J.J., 1988. Effect of rate sensitivity on the stability of torsion textures. Acta Metallurgica 36 (12), 3077–3091.

Tóth, L.S., Jonas, J.J., Neale, K.W., 1990. Comparison of the minimum plastic spin and rate sensitive slip theories for loading of symmetrical crystal orientations. Proceedings of the Royal Society of London A 427, 201–219.

Van der Giessen, E., Wu, P.D., Neale, K.W., 1992. On the effect of plastic spin on large strain elastic–plastic torsion of solid bars. International Journal of Plasticity 8, 773–801.

Van Houtte, P., 2002. Fast calculation of average Taylor factors and Mandel spins for all possible strain modes. International Journal of Plasticity 17, 807–818.

Vreeland Jr., T., 1968. Dislocation velocity in copper and zinc. In: Rosenfield, A.R., Hahan, G.T., Bement, A.L., Jaffee, R.I. (Eds.), Dislocation Dynamics. McGraw-Hill, New York, pp. 529–549.